Steel and Composite Structures, Vol. 6, No. 2 (2006) 123-138
DOI: http://dx.doi.org/10.12989/scs.2006.6.2.123

Construction sequence modelling of continuous steel-concrete composite bridge decks

Luigino Dezi† and Fabrizio Gara‡

Department of Architecture, Construction and Structures, Marche Polytechnic University, via Brecce Bianche 60131, Ancona, Italy

Graziano Leoni‡†

PROCAM, University of Camerino, Viale della Rimembranza, 63100, Ascoli Piceno, Italy

(Received February 3, 2005, Accepted October 19, 2005)

Abstract. This paper proposes a model for the analysis of the construction sequences of steel-concrete composite decks in which the slab is cast-in-situ for segments. The model accounts for early age shrinkage, such as thermal and endogenous shrinkage, drying shrinkage, tensile creep effects and the complex sequences of loading due to pouring of the different slab segments. The evolution of the structure is caught by suitably defining the constitutive relationships of the concrete and the steel reinforcements. The numerical solution is obtained by means of a step-by-step procedure and the finite element method. The proposed model is then applied to a composite deck in order to show its potential.

Keywords: steel-concrete composite decks; fractionated casting; construction sequence; shrinkage and creep effects; finite element method.

1. Introduction

In the construction of long continuous steel-concrete composite viaducts, the slab is poured in segments. A simple and rapid technique often used consists of leaning the pre-fabricated reinforcements on longitudinal steel girders and then concreting on formworks travelling on the unpropped steel girders (Dezi and Niccolini 2003).

During construction, the pouring of new slab segments not only modifies the geometry of the resistant cross section, which becomes composite only after concrete end-setting, but also the dead-load distribution on the structure. In fact, at time of pouring (t_p) the slab weight and the travelling formwork weight induce a stress state on the existing structure (Fig. 1a). Subsequently, during setting, the concrete heats up due to the hydration of the cement and then, after end-setting ($t \geq t_{es}$), the concrete rapidly cools thus reducing the volume (thermal shrinkage). At the same time, an endogenous shrinkage

†Full Professor, Corresponding author, E-mail: dezi@univpm.it
‡Assistant Professor
‡†Associate Professor

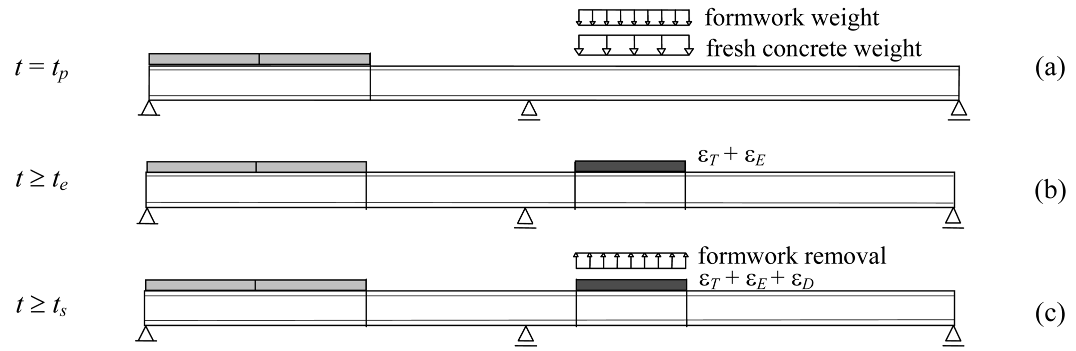

Fig. 1 Construction sequences: actions during to the construction of one slab segment

component develops during concrete hardening due to the chemical reactions in the cement. Thermal shrinkage has a duration of about one week while endogenous shrinkage develops for few months after end-setting. Such early shrinkage components are restrained by the steel beams and the reinforcements and generate significant tensile stresses in the concrete that has not yet reached the final tensile strength (Fig. 1b). Successively, when the formwork is removed, the deck section is unloaded. From this instant (t_s), the drying shrinkage component adds to the other components (Fig. 1c), growing in time.

As a consequence of the construction phases and the early shrinkage, significant tensile stresses may arise in the young concrete that may crack because of its low tensile strength. The phenomenon of early cracking was pointed out in American and European reports (Krauss and Rogalla 1996, SETRA 1995, Ducret and Lebet 1999) where the results of monitoring carried out on a large number of bridges during the constructive phases were presented. In many cases patterns of full depth cracks were observed during construction even on the sagging regions where the concrete is usually considered to be uncracked.

Despite the importance of the problem, few models studying the effects of the slab casting sequence, are available in literature. Marì (2000) proposed a numerical model for the non-linear and time dependent analysis of both concrete and steel-concrete composite frames which takes into account the effects of the changes of the longitudinal scheme and the cross section during the construction process. Kwak *et al.* (2000) developed a model for the non-linear and time dependent analysis of steel-concrete composite girders evaluating the effects of the slab casting sequences and of the drying shrinkage in composite bridge decks. Such models permit following the time dependent behaviour of the structure in a very sophisticated manner accounting for concrete cracking. This is crucial for the prediction of the behaviour of bridges since concrete cracking may deeply affect the deformability and the stress distributions. Marì *et al.* (2003) proposed a study on the effects of construction process and slab prestressing on the serviceability behaviour of composite bridges. Four kinds of deck casting were studied for a short span continuous bridge but attention was focused almost exclusively on the long term behaviour while the behaviour of the deck during construction was not investigated accurately.

The authors have recently discussed the problem of the time-dependent behaviour of continuous composite decks with fractionated slab casting taking into account the flexibility of the shear connection and early-age shrinkage (Dezi *et al.* 2003). They focused attention on the tendency of the concrete slab to undergo early cracks by also showing that the slab longitudinal normal stresses are always tensile stresses. This suggests the use of a suitable creep function for time-dependent analyses.

The aim of this paper is to propose a model to investigate the causes of premature slab cracking, namely early concrete shrinkage and the slab casting sequence, and to design practical methods to prevent (or at least minimize) such early cracking. A finite element model for the analysis of the construction sequences in steel-concrete composite bridges is proposed. An analytical treatment of the problem and a relevant numerical procedure, based on the finite element method and a step-by-step procedure, are presented. The procedure is based on constitutive linear elastic relationships for the steel and linear viscoelastic relationships of the concrete; concrete cracking is disregarded. This is a limitation of the model that furnishes only a rough approximation of the structure behaviour when the slab is cracked. Nevertheless, in the case of optimised sequences of casting, for which the concrete does not reach the tensile strength, the model furnishes precious information on the behaviour of the bridge during construction.

Finally, an application to a real bridge is proposed in order to show the potential of the model which allows following the complex time history of the stresses due to the progressive loading of the structure, as well as the development of shrinkage and creep redistributions.

2. Analytical model

Reference is made to the composite deck shown by Fig. 2, with a tapered steel beam. In order to analyse the slab casting sequences, the girder is subdivided into n_{bs} sections each characterised by its own instant of concrete pouring (t_p). The reference frame $\{0; X, Y, Z\}$ is chosen as in Fig. 2, with the co-ordinate plane XZ at the beam-slab interface.

The kinematical model of a composite beam with flexible shear connection, proposed by Newmark *et al.* (1951), is adopted; in other words, the preservation of the plane cross section is considered separately for the concrete slab and the steel beam while the same vertical displacement is assumed for the two parts. By neglecting the shear deformability of the beam and the slab, the two conditions are translated mathematically by the following equations

$$v(x, y, z;t) = v_0(z;t) \tag{1}$$

$$w_s(x, y, z;t) = w_{s0}(z;t) - yv_0'(z;t) \tag{2}$$

$$w_c(x, y, z;t) = w_{c0}(z;t) - yv_0'(z;t) \tag{3}$$

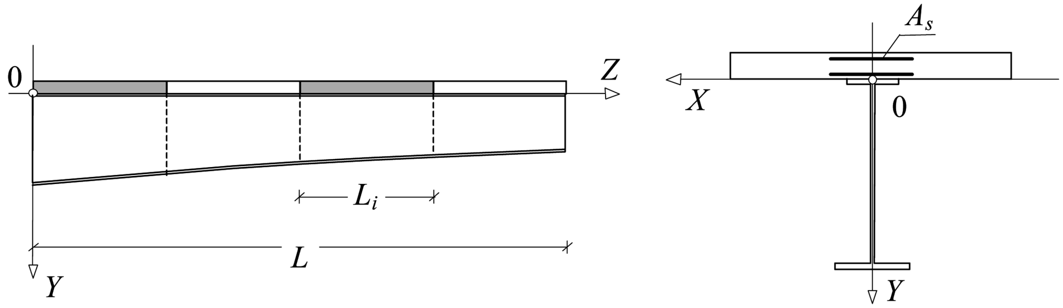

Fig. 2 Beam geometry and reference system frame

where t is the generic instant of the analysis, v_0 is the vertical displacement of the composite cross section and w_{s0} and w_{c0} are the longitudinal displacements of the steel beam and of the concrete slab measured at the points positioned on the beam-slab interface, respectively. Consequently, the interface slip Γ between the slab and the beam assumes the following expression:

$$\Gamma(z;t) = w_{s0}(z;t) - w_{c0}(z;t) \tag{4}$$

It is important to note that the analytical description of the problem in question, characterized by concrete slab sections having different casting times, requires a geometrical domain which includes all the slab sections, even those which have not yet been poured and the slab displacement field is defined even where the steel beam is alone. Consequently, while the structural continuity of the steel beam implies the regularity of the two functions w_{s0} and v_0, w_{c0} is discontinuous at the interface cross sections between the adjacent slab segments. In these cross sections only the increments of all the functions are regular after concrete end-setting of the adjacent slab segments.

Finally, from Eqs. (1-3) the following non-zero components of the strain tensor can be calculated:

$$\varepsilon_s(x, y, z;t) = w'_{s0}(z;t) - yv''_0(z;t) \tag{5}$$

$$\varepsilon_c(x, y, z;t) = w'_{c0}(z;t) - yv''_0(z;t) \tag{6}$$

2.1. Constitutive relationships

Linear constitutive relationships are considered for the various elements (steel beam, shear connectors, concrete and reinforcements) because during construction the yield limits of the materials should not be exceeded. Furthermore, concrete cracking is disregarded because it does not affect the results in the cases in which optimised sequential castings are considered. In fact, as will be shown in the following sections, in those cases during construction the concrete stresses are lower than the concrete tensile strength. This is obviously a limitation for the model because it cannot correctly predict the behaviour when concrete cracking occurs as in the case of continuous casting. Also, the model cannot describe the behaviour of the deck under service conditions where traffic loads and drying shrinkage induce concrete cracking. However, as already stated, the spirit of this research is to propose a model capable of catching the effects of the concrete rheology at early ages in order to properly optimise the slab casting sequence.

As stated in the previous section, the slab and the relevant reinforcements are considered geometrically even when the slab has not yet been poured and the change of the structural scheme is introduced by suitably defining the concrete constitutive law. For the concrete slab the following constitutive relationship is considered:

$$\sigma_c(t) = H(t - t_{es})\left\{\frac{[\varepsilon_c(t) - \varepsilon_c(t_{es}) - \bar{\varepsilon}(t)]}{J_p(t, t)} + \int_{t_{es}}^{t} \frac{\sigma_c(\tau)}{J_p(t, t)} \frac{\partial J_p(t, \tau)}{\partial \tau} d\tau\right\} \tag{7}$$

where H $(t - t_{es})$ is the Heavyside function (zero for $t < t_{es}$ and equal to one for $t \geq t_{es}$) and ε_c (t_{es}) is the concrete strain at the end-setting time t_{es}. This last term plays the role of a fictitious non mechanical strain so that the stress state is related only to the strain that develops after concrete end-setting. Furthermore, $\bar{\varepsilon}$ is the cumulative strain due to endogenous, thermal and drying shrinkage. Finally, J_p is the creep function of the concrete poured at time t_p, namely the strain at time t due to a unit stress applied at time and maintained constant in time. Notice that, according to this standard definition, $J_p(t,t)^{-1}$ is equal to the concrete Young's modulus at time t of the concrete poured at time t_p and thus Eq. (7) permits catching the variability in time of the concrete Young modulus and the effects of instantaneous loadings.

Analogously, the stress in the reinforcing steel is given by

$$\sigma_r(t) = H(t-t_{es})E_r[\varepsilon_c(t) - \varepsilon_c(t_{es})] \tag{8}$$

where E_r is the relevant Young modulus.

For the steel beam and the shear connection, which is considered spread along the beam, the classic linear elastic relationships hold

$$\sigma_s(t) = E_s\varepsilon_s(t) \tag{9}$$

$$q(t) = \rho\Gamma(t) \tag{10}$$

where E_s is the steel Young modulus and ρ is the stiffness per unit length of the shear connection.

2.2. Equilibrium condition

The solving equilibrium condition is obtained by the Virtual Work Theorem valid for three-dimensional bodies

$$\int_V \boldsymbol{S}\cdot\nabla(\delta\boldsymbol{u}) = \int_V \boldsymbol{b}\cdot\delta\boldsymbol{u} + \int_{\partial V}\boldsymbol{f}\cdot\delta\boldsymbol{u} \qquad \forall\delta\boldsymbol{u}\neq\boldsymbol{0} \tag{11}$$

where $\boldsymbol{S}$ is the Cauchy symmetric stress tensor, $\delta\boldsymbol{u}$ is the variation of the displacement field, ∇ is the gradient operator, $\boldsymbol{b}$ and $\boldsymbol{f}$ are the body and the surface forces applied to the structure, respectively. By taking into account the displacements, and the strains previously defined (Eqs. 1-6) as well as the constitutive relationships (7-10), the integrals in Eq. (11) may be written as the summation of various terms each related to a homogeneous section. In particular, as a consequence of the displacement field chosen (Eqs. 1-3), the integrals can be carried out on the cross section leading to the equation

$$\sum_{n_{bs}}\int_{L_i}\{\boldsymbol{K}_s + H(t-t_{es})[\boldsymbol{K}_c(t)+\boldsymbol{K}_r]\}\,\mathcal{D}\boldsymbol{s}(t)\cdot\mathcal{D}\delta\boldsymbol{s}dz$$

$$\sum_{n_{bs}}\int_{L_i}\left\{\boldsymbol{p}(t)\cdot\mathcal{H}\delta\boldsymbol{s}+H(t-t_{es})[E_{cp}(t)\bar{\varepsilon}(t)+(\boldsymbol{K}_c(t)+\boldsymbol{K}_r)\mathcal{D}\boldsymbol{s}(t_{es}) - \int_{t_{es}}^{t}\boldsymbol{f}_c(\tau)E_{cp}(t)\frac{\partial J_p(t,\tau)}{\partial\tau}d\tau]\cdot\mathcal{D}\delta\boldsymbol{s}\right\}dz$$

$$\forall\delta\boldsymbol{s}\neq\boldsymbol{0} \tag{12}$$

where $\boldsymbol{s} = [w_{s0}\ w_{c0}\ v_0]^T$ is the vector of the unknown displacements, $E_{cp}(t) = J_p(t,t)^{-1}$ is the concrete Young modulus at time t of the concrete poured at time t_p and $\boldsymbol{K}_s$, $\boldsymbol{K}_c$ and $\boldsymbol{K}_r$ are the stiffness matrix components. The first refers to the steel beam and the shear connection, the second to the concrete and the third to the reinforcements; these are given by the relations

$$\boldsymbol{K}_s = \begin{bmatrix} E_sA_s & 0 & E_sS_s & 0 & 0 \\ 0 & 0 & 0 & 0 & 0 \\ E_sS_s & 0 & E_sI_s & 0 & 0 \\ 0 & 0 & 0 & \rho & 0 \\ 0 & 0 & 0 & 0 & \rho \end{bmatrix} \quad \boldsymbol{K}_c(t) = E_{cp}(t)\begin{bmatrix} 0 & 0 & 0 & 0 & 0 \\ 0 & A_c & S_c & 0 & 0 \\ 0 & S_c & I_c & 0 & 0 \\ 0 & 0 & 0 & 0 & 0 \\ 0 & 0 & 0 & 0 & 0 \end{bmatrix} \quad \boldsymbol{K}_r = E_r\begin{bmatrix} 0 & 0 & 0 & 0 & 0 \\ 0 & A_r & S_r & 0 & 0 \\ 0 & S_r & I_r & 0 & 0 \\ 0 & 0 & 0 & 0 & 0 \\ 0 & 0 & 0 & 0 & 0 \end{bmatrix} \tag{13,14,15}$$

Furthermore, $\boldsymbol{f}_c = \begin{bmatrix} 0 & N_c & M_c & 0 & 0 \end{bmatrix}^T$ is the vector grouping the stress resultants in the concrete, $\bar{\varepsilon} = \bar{\varepsilon}\begin{bmatrix} 0 & A_c & S_c & 0 & 0 \end{bmatrix}^T$ is the vector grouping terms related to the shrinkage and $\boldsymbol{p} = \begin{bmatrix} p_{zs} & p_{zc} & p_y & m \end{bmatrix}^T$ is the vector of the resultants of the applied external forces. Finally $\mathscr{D}$ and $\mathscr{H}$ are the formal differential operators defined as

$$\mathscr{D}^T = \begin{bmatrix} \partial & 0 & 0 & 1 & 0 \\ 0 & \partial & 0 & 0 & -1 \\ 0 & 0 & -\partial^2 & 0 & 0 \end{bmatrix} \qquad \mathscr{H}^T = \begin{bmatrix} 1 & 0 & 0 & 0 \\ 0 & 1 & 0 & 0 \\ 0 & 0 & 1 & -\partial \end{bmatrix} \tag{16, 17}$$

In the previous expressions A, S and I denote the area and the first and second moment of area, calculated with respect to the X axis, of the concrete part (c), the reinforcing steel (r) and the steel beam (s).

As earlier stated, Eq. (12) is written as the summation of the contributions given by the different homogeneous beam sections. The Heavyside function permits catching the evolution of the structure during construction by switching the contributions of the slab for the instants after concrete end-setting.

3. Numerical solution

The problem is defined in a time-space domain and the numerical solution of (12) must be sought accordingly by introducing a double discretization, the first for the time domain and the second for the beam axis. In the following sections the numerical procedures will be illustrated.

3.1. Time integration

Thanks to the time discretization, the time integrals can be approximated with the trapezoidal rule according to the formula

$$\int_{t_{es}}^{t} G(\tau)\frac{\partial J(t,\tau)}{\partial \tau}d\tau \cong \frac{1}{2}\sum_{i=1}^{n}[G(t_i) + G(t_{i-1})][J(t,t_i) - J(t,t_{i-1})] \tag{18}$$

where G is the generic function of t.

With reference to the n-th instant of the time discretization, the Virtual Work Theorem provides

$$\sum_{n_{bs}} \int_{L_i} \{\boldsymbol{K}_s + H(t_n - t_{es})[\boldsymbol{K}_{cn} + \boldsymbol{K}_r]\}\mathcal{D}\boldsymbol{s} \cdot \mathcal{D}\delta\boldsymbol{s}dz =$$
$$\sum_{n_{bs}} \int_{L_i} \left[\boldsymbol{p}_n \cdot \mathcal{H}\delta\boldsymbol{s} + H(t_n - t_{es})\left(E_{cn}\bar{\varepsilon}_n + (\boldsymbol{K}_{cn} + \boldsymbol{K}_r)\mathcal{D}\boldsymbol{s}_{es} - \sum_{i=1}^{n-1} \boldsymbol{f}_{ci} \frac{E_{cn}}{\hat{E}_{cni}}\right) \cdot \mathcal{D}\delta\boldsymbol{s}\right]dz \qquad \forall \delta\boldsymbol{s} \neq 0 \tag{19}$$

where

$$E_{cn} = 2[J_p(t_n, t_n) + J_p(t_n, t_{n-1})]^{-1} \qquad \hat{E}_{cni} = 2[J_p(t_n, t_{i+1}) - J_p(t_n, t_{i-1})]^{-1} \tag{20, 21}$$

are fictitious elastic constants of the concrete. In the expression, subscript n indicates quantities calculated at time t_n and $\boldsymbol{K}_{cn}=\boldsymbol{K}_c(t)E_{cn}/E_{cp}(t)$. Eq. (19) governs a sequence of pseudo-elastic problems which, thanks to a step-by-step procedure, gives the solution of the original problem for a finite number of instants (time mesh). The solution at each time depends on the current value of the external loads and on the non-mechanical strain of the concrete slab constituted by three components: shrinkage strain, strain developed before the end-setting of the slab, and creep strain due to the complete history of the concrete stresses. In particular the resultants of the concrete stresses are calculated by means of the recursive formula

$$\boldsymbol{f}_{ci} = \boldsymbol{K}_{ci}\mathcal{D}(\boldsymbol{s}_i - \boldsymbol{s}_{es}) - \bar{\varepsilon}_i E_{ci} + \sum_{j=1}^{i-1} \boldsymbol{f}_{cj} \frac{E_{ci}}{\hat{E}_{cij}} \tag{22}$$

It is worth noting that each slab segment is characterised by its own times of pouring (t_p) end-setting (t_{es}) and formwork removal (t_s) and the deck construction is regulated by the sequence of such events. The time mesh adopted must be chosen by subdividing each of the time intervals defined by two of these events into a number of sub intervals (n_t). In order to catch the evolution in time of the stresses, which is characterised by a high rate just after the application of the loads, the time mesh should be suitably refined. To obtain good results, the first step of analysis should be about 10^{-2} days while a geometrical sequence can be adopted for the other time intervals. In practice, the mesh of each time interval between two consequent events t_A and t_B can be obtained by the following numerical sequence:

$$\vartheta_0 = t_A \tag{23a}$$

$$\vartheta_1 = \vartheta_0 + 0.01 \tag{23b}$$

$$\vartheta_i = \vartheta_0 + 10^r(\vartheta_{i-1} - \vartheta_0) \qquad \text{for } i = 2,\dots, n_t \tag{23c}$$

where $r = [\log(t_B - t_A) - \log(\vartheta_1 - \vartheta_0)]/(n_t - 1)$.

3.2. Spatial integration

Thanks to the discretization of the beam axis, the finite element method can be used to solve the sequence of pseudo-elastic problems represented by Eq. (19). By subdividing the girder into a finite

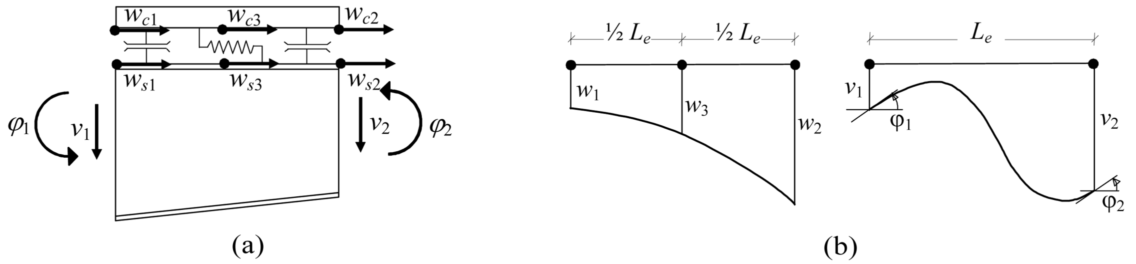

Fig. 3 10-*dof* finite element for composite beam with flexible shear connection: (a) nodal displacements; (b) interpolating functions

number of sub-domains (finite elements), the solution can be sought by approximating the unknown displacement functions according to the well known formula

$$\boldsymbol{s}_n(z) \cong \boldsymbol{N}_e(z)\boldsymbol{d}_{e_n} \tag{24}$$

where $\boldsymbol{N}_e$ is the matrix which groups the shape functions and $\boldsymbol{d}_{e_n}$ is the vector of the element nodal displacements at time t_n. In this case a refined 10 *dof* element (Fig. 3a) is adopted in which the displacement field is described by the vector

$$\boldsymbol{d}_{e_n} = \begin{bmatrix} w_{c1} & w_{s1} & v_1 & \varphi_1 & w_{c2} & w_{s2} & v_2 & \varphi_2 & w_{c3} & w_{s3} \end{bmatrix}^T \tag{25}$$

which groups the end vertical displacements, the end rotations, the axial displacements of the steel beam and of the concrete slab measured at the beam ends and at an intermediate node. The following interpolating polynomial of degree 3 is used for the vertical displacement v_0, while interpolating polynomials of degree 2 are used for the longitudinal displacements w_{c0} and w_{s0} (Fig. 3b).

$$N_{v1} = 1 - 3\lambda^2 + 2\lambda^3 \qquad N_{v2} = L_e(\lambda - 2\lambda^2 + \lambda^3) \tag{26a,b}$$

$$N_{v3} = 3\lambda^2 - 2\lambda^3 \qquad N_{v4} = L_e(-\lambda^2 + \lambda^3) \tag{26c,d}$$

$$N_{w1} = 1 - 3\lambda + 2\lambda^2 \qquad N_{w2} = -\lambda + 2\lambda^2 \qquad N_{w3} = -4\lambda + 4\lambda^2 \tag{26e,f,g}$$

in which L_e is the finite element length while $\lambda = z/L_e$ is the non-dimensional abscissa. The matrix grouping the shape functions becomes

$$\boldsymbol{N}_e = \begin{bmatrix} 0 & N_{w1} & 0 & 0 & 0 & N_{w2} & 0 & 0 & 0 & N_{w3} \\ N_{w1} & 0 & 0 & 0 & N_{w2} & 0 & 0 & 0 & N_{w3} & 0 \\ 0 & 0 & N_{v1} & N_{v2} & 0 & 0 & N_{v3} & N_{v4} & 0 & 0 \end{bmatrix} \tag{27}$$

It is worth underlining that measuring the longitudinal displacements of the slab and of the steel beam at the beam-slab interface is a particularly appropriate choice for the analysis of decks with steel beams having variable geometry. This element in fact permits solving problems in which the steel beam

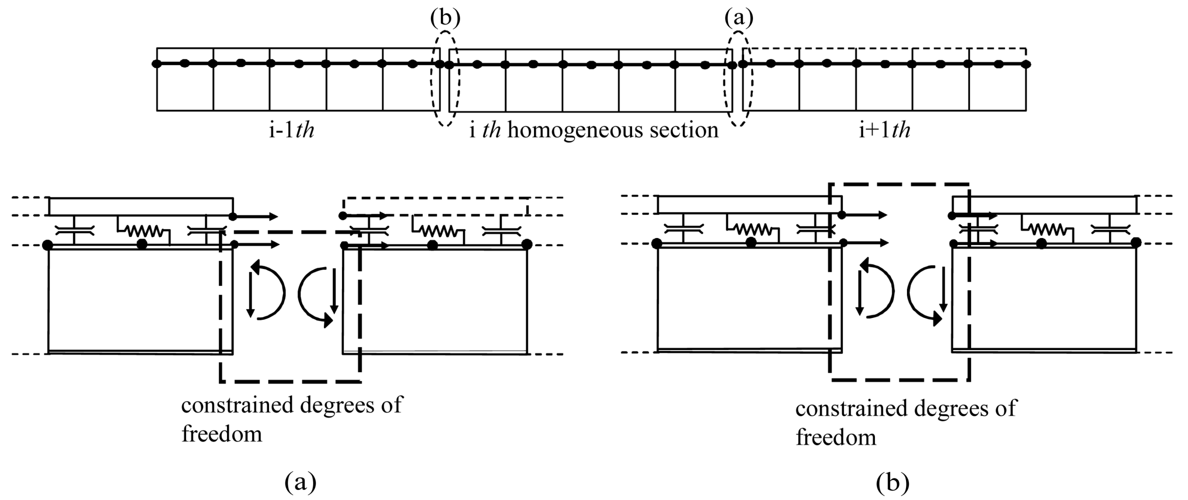

Fig. 4 Constraint between adjacent homogeneous sections: (a) between two sections before the end-setting; (b) between two sections after the slab end-setting

undergoes sudden variations of the plate thickness and of the flange width without introducing artifices (i.e., the definition of rigid body constraints) in assembling the stiffness matrix of the entire structure.

In order to catch the discontinuity of the functions describing the axial slab displacements, twin nodes are introduced at the cross sections separating the n_{bs} girder sections (Fig. 4). The longitudinal displacements of the slab, measured at the two nodes, will not depend on each other for instants before the concrete end-setting in both the adjacent slab sections. For the subsequent times, the displacement increments will be constrained (Fig. 4b). It is worth noticing that the constraint is applied to the displacements, and not to their increments. This is done by imposing that the difference of the displacements of the twin nodes be constant in time and equal to the relative displacement obtained at the time at which the constraint has become effective.

By substituting Eq. (24) into Eq. (19) the following equilibrium condition is obtained:

$$\boldsymbol{K}_n \boldsymbol{d}_n = \boldsymbol{f}_n^p + \boldsymbol{f}_n^{sh} + \boldsymbol{f}_n^e + \boldsymbol{f}_n^c + \boldsymbol{f}_n^r \tag{28}$$

where $\boldsymbol{d}_n$ is the following vector grouping the unknown nodal displacements at time t_n:

$$\boldsymbol{d}_n = \mathrm{b}_{i}^{n_{bs}} \; \mathrm{d}_{e}^{el,i} \; \boldsymbol{d}_{e_n} \tag{29}$$

where d is the assembling operator of the nodal displacement which operates on the elements of the same homogeneous girder section and b is the operator which constrains the degrees of freedom of the joints at the interface between the adjacent homogeneous girder sections as previously described.

The global stiffness matrix $\boldsymbol{K}_n$ is obtained by assembling the element stiffness matrixes according to the relation

$$\boldsymbol{K}_n = \mathrm{C}_{i}^{n_{bs}} \; \mathrm{A}_{e}^{el,i} \left\{ \int_{l_e} (\mathscr{D}\boldsymbol{N}_e)^T [\boldsymbol{K}_s + H(t_n - t_{es})(\boldsymbol{K}_{cn} + \boldsymbol{K}_r)](\mathscr{D}\boldsymbol{N}_e)\, dz \right\} \tag{30}$$

where A is the operator which assembles the element of the i-th homogeneous section while C is the operator which condenses the stiffness matrix according to the constraint between the adjacent homogeneous sections. Notice that the Heavyside function acts as a switch for the concrete slab and the steel reinforcements for the times $t_n - t_{es}$. Furthermore, while components $\boldsymbol{K}_s$ and $\boldsymbol{K}_r$ are the same for each step of the analysis, $\boldsymbol{K}_{cn}$ needs to be updated at each step.

Finally, $\boldsymbol{f}_n^p$, $\boldsymbol{f}_n^{sh}$, $\boldsymbol{f}_n^e$, $\boldsymbol{f}_n^c$ and $\boldsymbol{f}_n^r$ are the components of the nodal force vector and are related to the external loads, shrinkage, the non-mechanical strain accounting for the time evolution of the structural geometry, the concrete creep effects and the constraint applied to the relative displacement of the twin nodes, respectively. They assume the following expressions:

$$\boldsymbol{f}_n^p = \underset{i}{\overset{n_{bs}}{\mathsf{C}}}\ \underset{e}{\overset{el,i}{\mathsf{a}}} \int_{l_e} (\mathcal{H}\boldsymbol{N}_e)^T \boldsymbol{p}_n dz \tag{31}$$

$$\boldsymbol{f}_n^{sh} = \underset{i}{\overset{n_{bs}}{\mathsf{C}}}\ \underset{e}{\overset{el,i}{\mathsf{a}}}\ H(t_n - t_{es}) \int_{l_e} (\mathcal{H}\boldsymbol{N}_e)^T E_{cn}\bar{\varepsilon}_n dz \tag{32}$$

$$\boldsymbol{f}_n^e = \underset{i}{\overset{n_{bs}}{\mathsf{C}}}\ \underset{e}{\overset{el,i}{\mathsf{a}}}\ H(t_n - t_{es}) \int_{l_e} (\mathcal{D}\boldsymbol{N}_e)^T (\boldsymbol{K}_{cn} + \boldsymbol{K}_r)(\mathcal{D}\boldsymbol{N}_e)\boldsymbol{d}_{e_{es}} dz \tag{33}$$

$$\boldsymbol{f}_n^c = -\underset{i}{\overset{n_{bs}}{\mathsf{C}}}\ \underset{e}{\overset{el,i}{\mathsf{a}}}\ H(t_n - t_{es}) \int_{l_e} (\mathcal{D}\boldsymbol{N}_e)^T \sum_{i=1}^{n-1} \frac{E_{cn}}{\hat{E}_{cni}} \boldsymbol{f}_{ci} dz \tag{34}$$

$$\boldsymbol{f}_n^r = -\underset{i}{\overset{n_{bs}}{\mathsf{C}}} \left\{ \underset{e}{\overset{el,i}{\mathsf{A}}} \left\{ \int_{l_e} (\mathcal{D}\boldsymbol{N}_e)^T [\boldsymbol{K}_s + H(t_n - t_{es})(\boldsymbol{K}_{cn} + \boldsymbol{K}_r)](\mathcal{D}\boldsymbol{N}_e) dz \right\} \boldsymbol{r} \right\} \tag{35}$$

Similarly to the previous cases, a is the assembling operator of the elements of the same homogeneous section and c is the operator which condenses the nodal forces dual of the constrained degrees of freedom. Once again, the Heavyside function switches the contributions of the slab for times subsequent to the end-setting of the concrete. Finally, vector $\boldsymbol{r}$ appearing in Eq. (35) groups the slab relative displacements, between the twin nodes placed at the interface of the different homogeneous sections, which are constrained to be constant in time as previously described. In particular its components are all null except those corresponding to the displacement already constrained.

The numerical procedure makes it possible to catch the evolution of the complex static scheme due to the constructive phases and permits following the complete time evolution of displacements, stresses and shear flow at the beam-slab interface. The results may be organised in diagrams such as envelopes of maximum stresses obtained in the slab during construction or the stresses in each slab section for a fixed age of concrete. This gives a ready interpretation in order to establish the cracking tendency of the concrete slab.

The proposed method was validated by comparing the results with those furnished by models already proposed by the authors who studied the long-term behaviour of composite decks in a number of cases of practical interest (e.g., Dezi and Tarantino 1993, Dezi *et al.* 1995). The results of such analyses are not reported in this paper for the sake of brevity because curves obtained in the cases examined are perfectly superimposed and do not add any interesting information for the reader. However, the method was successfully applied to study the optimal sequential castings of composite bridge decks recently constructed in Italy (Dezi and Niccolini 2003).

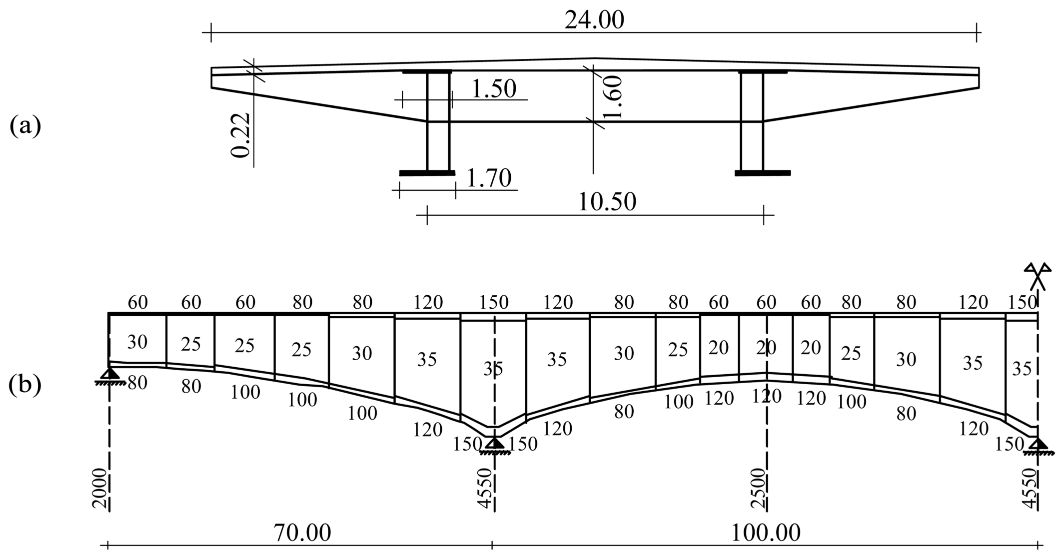

Fig. 5 Deck geometry: (a) cross section; (b) longitudinal view of the steel beam and sheet thickness scheme (in mm)

4. Application to a real deck

The model presented is applied to a realistic four span composite deck (70-100-100-70 m) with slab width of 24 m (Fig. 5). The two steel beams have a depth varying from a minimum of 2.00 m, at the end cross sections, to a maximum of 4.55 m over the two central supports, and 2.50 m at the intermediate spans, according to parabolic profiles as shown in Fig. 5(b). The web and flange thicknesses are also shown in Fig. 5(b). The slab has a constant thickness of 0.22 m and a geometric reinforcement ratio of 1%, in the span sections, and 2% in the inner support sections.

The slab is poured by means of travelling formworks having a self-weight of 540 kN. Two casting schemes are considered: a continuous sequence in which the formwork travels from one end to the other end of the deck (Fig. 6a) and an optimised scheme following the casting sequences shown by Fig. 6(b).

For each slab section the following external actions are considered: at the instant of concrete pouring, the slab and the formwork weights are applied to the steel beams; subsequently, after 1.5 days, a negative load is applied to the composite cross section to simulate the removal of the formwork. In order to remove the formwork after such a short time, a concrete with a strength of 20 MPa at 1 day is required. This means that, according to the relationship suggested by the CEBFIB (1988) Model Code 1990, strength at 28 days should be f_{ck} = 45 MPa.

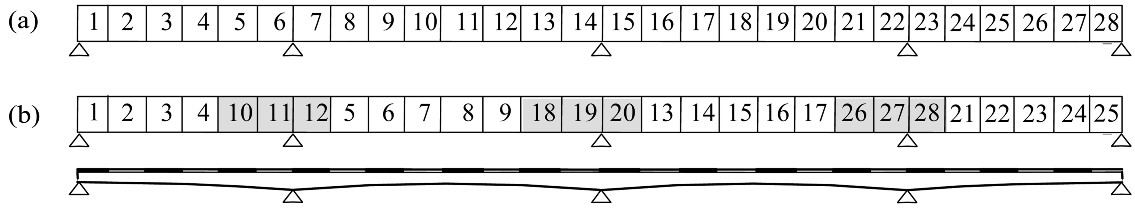

Fig. 6 Slab casting schemes: (a) continuous casting; (b) optimised sequential casting

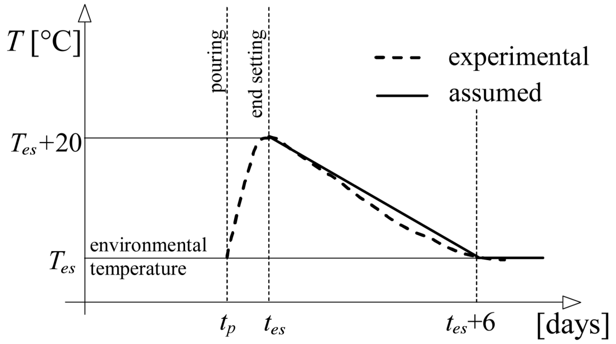

Fig. 7 Concrete cooling after end-setting

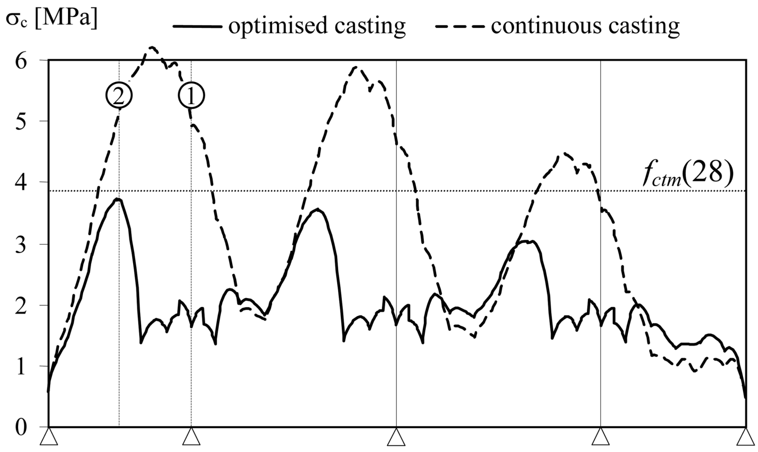

Fig. 8 Concrete stresses during constructive phases: envelopes of the maximum values

The time-dependent analysis is performed by considering the creep and drying shrinkage functions suggested by the CEB-FIP (1988) Model Code 1990 assuming RH = 75%. Endogenous shrinkage is disregarded while thermal effects due to cement hydration are estimated on the basis of available laboratory test results (Ducret and Lebet 1999). In particular, a reduction in temperature of 20 °C is considered over a period of 6 days (Fig. 7) according to a linear law.

Fig. 8 shows the envelops of the stresses, measured at the concrete slab mid-plane, produced by continuous casting and by optimised casting during the construction of the slab. All the slab sections are affected by tensile stresses both in the case of continuous and optimised casting. This confirms the crack patterns that have been observed to develop along the whole concrete slab of many newly constructed bridges (Krauss and Rogalla 1996, SETRA 1995). The optimised casting nevertheless produces much lower tensile stresses than those produced by continuous casting especially at the hogging regions.

Fig. 9 shows the time evolution of the concrete slab for the cross sections over the first support (cross section 1) and for the cross section of the first span at which the maximum tensile strength is achieved in the case of optimised casting (cross section 2). The curve superimposed to the diagrams, showing the evolution of the tensile strength, is obtained by the relationship.

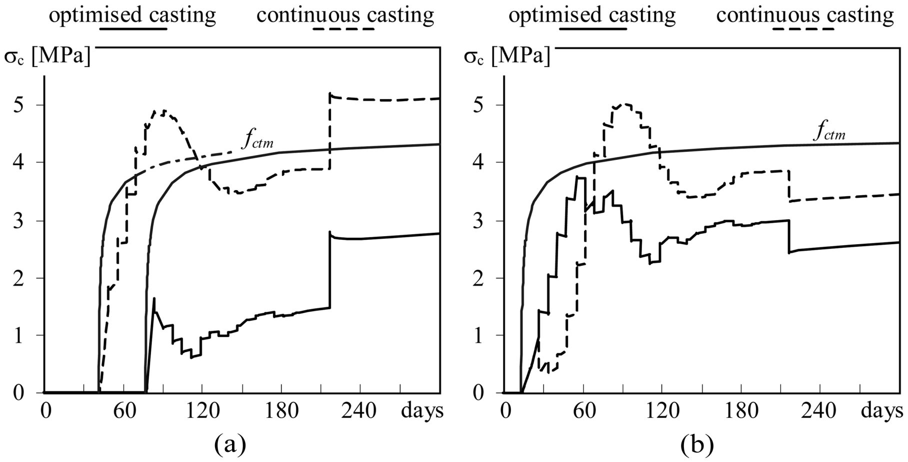

Fig. 9 Time evolution of concrete stresses: (a) cross section 1; (b) cross section 2

$$f_{ctm}(t) = 0.3 f_{ck}^{2/3} e^{0.20\left(1-\frac{5.3}{t^{0.5}}\right)} \tag{36}$$

derived with the CEB-FIP (1988) Model Code 1990 by considering the same time evolution of the concrete compression strength. In the case of continuous casting the stress exceeds the concrete strength in both the cross sections while for optimised casting the tensile strength is not reached.

Since the concrete tensile strength is exceeded by stresses, the case of continuous casting is not completely realistic because the model cannot catch concrete cracking; it may nevertheless be stated that in the cross sections where the stress is higher than the tensile strength there is a very high probability of crack formation during construction. By taking into account that the concrete tensile strength at 28 days is $f_{ctm} = 3.8$ MPa, it is possible to say that in the case of continuous casting there is a high probability that cracking will develop during construction in wide regions of the slab, as can be observed in Fig. 8.

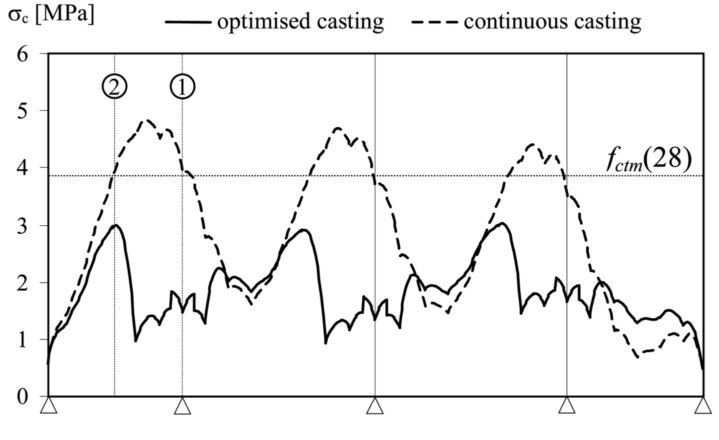

Fig. 10 Concrete stresses at the end of constructive phases

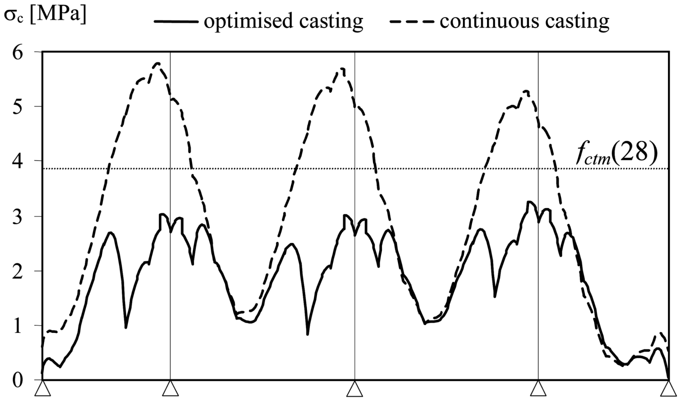

Fig. 11 Concrete stresses after the application of the dead load

Fig. 10 shows the stress diagram in the concrete slab a few weeks after complete slab pouring; on this residual stress state, additional stresses due to the pavement weight and traffic loads will be superimposed. It is evident that the reduction of the tensile stresses over the support obtained with optimised casting is particularly important to control cracking caused by the external loads which induce negative moments.

This is confirmed by Fig. 11 that shows the stress diagram in the concrete slab after the laying of the pavement. In the case of continuous casting the stress state augments by about 20% over the supports. Vice versa, in the case of optimised casting, the stress level augments only over the supports, so that the final distribution is almost uniform and the maximum values are similar to those of Fig. 10.

5. Conclusions

A model for the analysis of the constructive phases of continuous composite steel-concrete decks, in which slab segments are cast-in-situ by using travelling formworks leaning on un-propped steel beams, is proposed. The model catches the evolution of the structure that undergoes complicated changes of geometry during construction. It accounts for the following aspects:

- thermal shrinkage caused by the reduction in volume after the rise in temperature due to concrete setting and endogenous chemical shrinkage;
- drying shrinkage caused by the loss of humidity of the hardened concrete;
- concrete creep under tensile stresses;
- loading phases during the various construction stages of the slab (weight of the fresh concrete and formworks, removal of formworks);
- deformability of the shear connectors.

The model describes the behaviour of tapered steel beams and/or steel beams with varying geometry due to the changes of the steel sheets. The materials are considered in the linear range and concrete cracking is disregarded. These assumptions do not introduce approximations when studying optimised sequences of casting for which the concrete usually does not undergo cracking. Conversely, this represents a limitation of the model that is not reliable in predicting the behaviour of the structure in the long term, when concrete cracking occurs due to traffic loads and drying shrinkage.

The numerical solution was obtained with the finite element method and a step-by-step procedure. This makes it possible to follow the complex time evolution of the stress state due to the various actions and to the stress redistribution that develops as a consequence of the concrete creep.

The proposed model was applied to a real bridge deck, having variable-depth steel beam, in order to show its potential. Two different casting schemes, namely a continuous sequence from one end to the other end of the deck, and an optimised scheme where the slab sections in the spans are poured before those over the inner supports, were considered.

The following conclusions may be drawn from the application:

- the model catches the tensile stress patterns that develop during construction when the concrete tensile strength has not reached its maximum value; this result confirms the cracking tendency of concrete slabs during construction observed by Krauss and Rogalla (1996), SETRA (1995) and Ducret and Lebet (1999);
- the choice of the slab casting sequences assumes a fundamental role in limiting tensile slab stress during the construction phases;
- by using an optimised casting sequence, the tensile stresses on the concrete slab are much lower than those produced by a continuous sequence; stress reduction is more significant over the inner supports where additional tensile stresses are produced by the application of dead and service loads.

References

CEB-FIP Model Code 1990 (1988), "CEB Bulletin d'Information n. 190", CEB-FIP Comité Euro-International du Béton – Fédération International de la Précontrainte, Paris, France.

Dezi, L. and Tarantino, A. M. (1993), "Creep in composite continuous beams. I: Theoretical treatment", *J. Struct. Engrg.* ASCE, **119**(7), 2095-2111.

Dezi, L. Leoni, G. and Tarantino, A. M. (1995), "Time-dependent analysis of prestressed composite beams", *J. Struct. Engrg.* ASCE, **121**(4), 621-633.

Dezi, L., Gara, F., Leoni, G. and Vitali, A. (2003), "Slab cracking control in composite decks by means of fractionated castings", *Proc. of ASSCCA'03*, Sydney, Australia, 1029-1034.

Dezi, L. and Niccolini, S. (2003), "Les Viaducs de la Bretelle d'Urbino Italie", *Bulletin 22 Ponts Métalliques,* OTUA, 170-186.

Ducret, J. M. and Lebet, J. P. (1999), "Behaviour of composite bridges during construction", *Structural Engineering International*, **3**, 212-218.

Krauss, P. D. and Rogalla, E. A. (1996), *Transverse Cracking in Newly Constructed Bridge Decks*, National Academy Press, Washington, USA.

Kwak, H. G., Seo, Y. J. and Jung, C. M. (2000), "Effects of the slab casting sequences and the drying shrinkage of concrete slabs on the short-term and long-term behaviour of composite steel box girder bridges", *Eng. Struct.*, **23**, 1453-1480.

Marì, A. R. (2000) "Numerical simulation of the segmental construction of three dimensional concrete frames", *Eng. Struct.*, **22**, 585-596.

Marì, A. R., Mirambell, E. and Estrada, I. (2003) "Effects of construction process and slab prestressing on the serviceability behaviour of composite bridges", *J. Construct. Steel Res.*, **59**, 135-163.

Newmark, N. M., Siess, C. P. and Viest, I. M. (1951), "Tests and analysis of composites beams with incomplete interaction", *Proc. Soc. Exp. Stress Anal.*, **9**(1), 75-92.

SETRA (1995), *Recommandations pour maîtriser la fissuration des dalles*, SETRA, Bagneux, France.

Notation

In the sequel, the main symbols used in this paper are reported.

A : area
$\boldsymbol{b}$: body force
$\boldsymbol{d}_e$: vector of nodal displacements
$\mathscr{D}$, $\mathscr{H}$: differential operators
E : Young's modulus
E_{cn}, $\hat{E}_{cni}$: Fictitious elastic constants for the concrete
$\boldsymbol{f}$: surface force
$\boldsymbol{f}_c$: vector of the stress resultant in the concrete part;
H : heavyside function
I : second moment of area
J : creep function
$\boldsymbol{K}$: stiffness matrix
$\boldsymbol{N}_e$: matrix of the shape functions
m : moment
n : number of time step
$\boldsymbol{p}$: vector of the external loads
p_y : vertical load
p_{zc} : longitudinal load on the slab
p_{zs} : longitudinal load on the steel beam
q : shear flow at beam slab interface
S : first moment of area
$\boldsymbol{S}$: Cauchy's stress tensor
$\boldsymbol{s}$: generalised displacements vector
t : generic time
$\boldsymbol{u}$: displacement vector
v : vertical displacement
r : coefficient defined in Eqs. (23)
v_0 : vertical displacement of the composite cross section
w : longitudinal displacement
w_{c0}, w_{s0} : longitudinal displacements of the concrete slab and the steel beam at the beam-slab interface
x, y, z : coordinates
Γ : slip between steel beam and concrete slab
∇ : gradient
δ : variation
ε : longitudinal strain
ϑ : time of the discretization of the interval between two events
$\bar{\varepsilon}$: cumulative strains due to shrinkage
$\boldsymbol{\varepsilon}$: vector grouping terms related to shrinkage
ρ : stiffness per-unit-length of the shear connection
σ : longitudinal stress
τ : variable in the superposition integrals

Subscripts

c : concrete
e : finite element
es : end setting
i : index of time instant
n : index of time instant
p : pouring
r : reinforcements
s : steel
CC